Table 34. Mineral compositions used in matrix inversion to produce normative mineralogy logs (see Fig. 93).

Input coefficients	Actinolite	Plagioclase	Chlorite	Olivine	Clinopyroxene	Smectite
WPSI	0.53	0.49	0.28	0.38	0.55	0.49
WPAL	0.02	0.36	0.12	0.88	0.00	0.06
WPFE	0.15	0.02	0.21	0.00	0.22	0.12
WPMG	0.13	0.02	0.18	0.53	0.18	0.23
WPCA	0.13	0.13	0.00	0.06	0.10	0.01

waveforms of good quality were recorded with the MCS in Layers 2A, 2B, and 2C of Hole 504B. Preliminary interpretation shows that data recorded not only agree well with previous recording of elastic properties in this hole (Anderson, Honnorez, Becker, et al., 1985; Moos et al., 1986; Little and Stephen, 1985), but also allow for more detailed analysis owing to the better quality of data acquired with the MCS. Velocities computed with the semblance technique can be used to differentiate between flow, pillow, and brecciated units, and to study the effects of fracturing and alteration on elastic properties of basalts.

VERTICAL SEISMIC PROFILE EXPERIMENT

Introduction

A vertical seismic profile (VSP) experiment was conducted at DSDP Hole 504B (Anderson et al., 1982; CRRUST, 1982) to determine the detailed velocity-depth structure and reflection seismogram for crustal Layers 2, 3, and the upper mantle on the south flank of the Costa Rica Rift spreading center (Fig. 102). VSP measurements not only provide such seismic information for the reflection interfaces penetrated by the borehole, but they can also be used to predict the nature and depth to interfaces below total depth of the borehole (Gal'perin, 1974). Figure 103 shows a generalized, schematic representation of the ray paths and diverging wavetrain pattern for direct and reflected arrivals in a typical VSP experiment (Mons and Barbour, 1981).

Objectives

The primary objectives of the VSP experiment at Hole 504B were to: (1) determine the feasibility of using both air-gun and water-gun sound sources to obtain both deep penetration and high-resolution seismic reflections from interfaces as deep as the Mohorovicic discontinuity (Moho) boundary between Layer 3 and the upper mantle; (2) determine whether the specific drilling target horizon for Leg 111, the boundary between the closely spaced reflector sequence of Layer 2 and the widely spaced dipping reflectors of Layer 3 at about 5600 ms (two-way traveltime) on the MCS line RC-485 (Fig. 104), was actually within reach of the drill bit. The boundary was estimated to be about 2 km below seafloor or 5.46 km below sea level; (3) determine the detailed direct wave velocity-depth profile and vertical reflection seismogram of the Layer 2A, 2B, and 2C sequence and the interface between Layer 3 and the Moho; (4) precisely relate the seismic profile to the borehole lithology and other logging information in order to determine the physical origin of the Layer 2 reflector sequence; and (5) correlate the VSP reflection seismogram with the surface MCS lines which characterize the regional structure framework for Hole 504B (T. Brocher and J. M. Mutter, pers. comm., 1986).

Unfortunately, objective (1) could not be fully achieved due the almost immediate failure of the large water gun, the high-frequency sound source originally planned for the experiment. A much smaller water gun, substituted at the last minute, did not have adequate signal strength to even penetrate the oceanic basement! However, the large air-gun sound source clearly demonstrated that vertical reflections can be observed from interfaces as deep as the Moho and perhaps deeper. Virtually all of objectives (2) and (3) were accomplished during the cruise. However, objectives (4) and (5) will require more extensive computer studies ashore before they can be fully realized.

Method

The sound sources originally planned for the Hole 504B VSP experiment were a large-volume (950 in.^{3}/16.0 L), high-pressure (2000 psi/106 bar) air gun (Bolt Model 1500C) on loan from Bedford Institute of Oceanography (Canada) and the *Resolution*'s large-volume (400 in.^{3}/4.0 L), high-pressure (2000 psi/106 bar) water gun (SSI P400 Model 02). These guns were suspended, one above the other from a buoy at 4.5 and 2.5 mbsl, respectively (Fig. 105). The buoy suspending the guns was tethered from the drillship's aft port crane boom about 24.4 m abeam (Fig. 106). The guns were not fired together. Alternate shooting schedules were maintained, which actually resulted in two separate VSP experiments being performed. Comparison tests shots with both guns in place and with each gun alone showed that the passive gun had little shadowing effect on the shooting gun. The most significant effect noted was a slight increase ($\sim$5%) in the peak pressure of the air gun's downward radiated pulse and a similar decrease in the water gun's peak pressure pulse. No appreciable change was observed in the guns' primary or bubble pulse frequencies.

The water-gun/air-gun selection and operating depth were decided after a series of test firings over a range of depths using several different guns. Figure 107 shows the test results for the SSI 400-in.^{3} water gun and the Bolt 1500C air gun fitted with a 487-in.^{3} chamber with debubbler. Figure 108 shows the results for the Bolt 1500C air gun fitted with 300-in.^{3} and 950-in.^{3} chambers without debubblers. Figures 109 and 110 summarize the primary pulse performance characteristics for all the guns. Careful scrutiny of these figures show that the 400-in.^{3} water gun and the 950-in.^{3} air gun produce primary pulse peak pressures at 125 and 47 Hz at the gun firing depth selected for this experiment (2.5 and 4.5 m, respectively). Also, the low frequency (6 Hz) bubble pulse amplitude of the 950-in.^{3} air gun appears to peak at about 4–5 m depth. Unfortunately, malfunction of the 400-in.^{3} water gun required substitution of a much smaller, untested 80-in.^{3} water gun (SSI S80 Model) at the preset depth (2.5 m) of the larger water gun. The primary pulse peak pressure and frequency of the 80-in.^{3} water gun at 2.5 m depth is also plotted with the large water gun's test data (Fig. 107). Clearly the small water gun produced a much weaker but higher frequency primary pulse than the large 400-in.^{3} water gun. This probably accounts for the much lower signal-to-noise (S/N) ratio of the small water gun during the actual VSP experimental results which are described later.

The downhole seismic signals were received with a Schlumberger Well Seismic Tool (WST) single vertical component seismometer. The seismometer had four series-connected 10 Hz (F_0) geophones (Geospace Model HS-1) mounted at its base (Fig. 111). Two complete WST seismometers were made available for

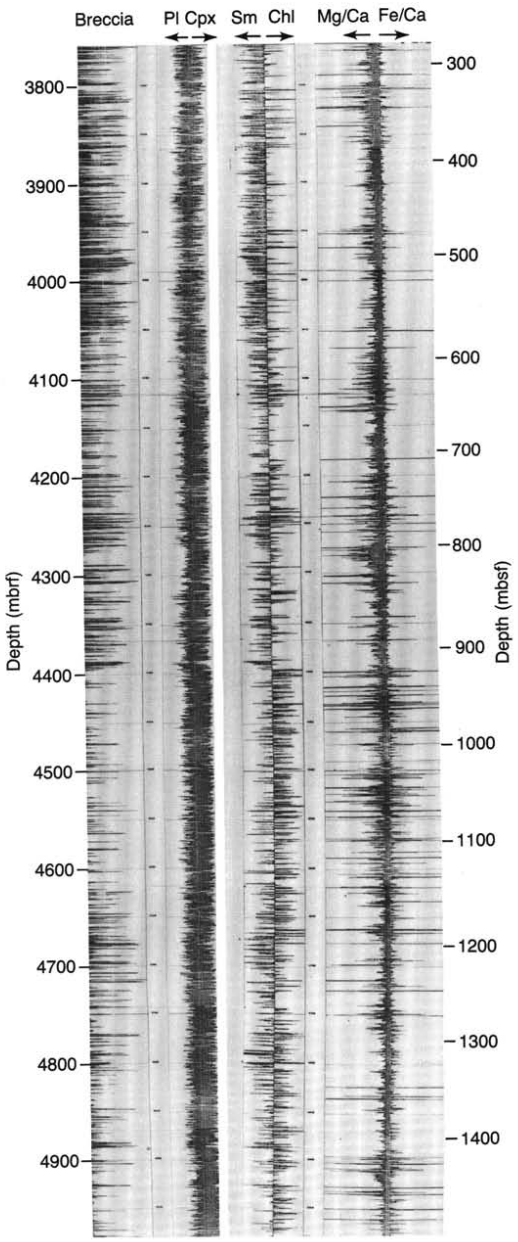

Figure 94. Breccia abundance (left) from mineralogical inversion of elemental logs (see Plate 6 for components). Plagioclase, clinopyroxene, smectite, and chlorite abundances (center) calculated in same way. Mg and Fe variations relative to Ca (right).

this experiment to allow quick substitution in the event of equipment malfunction. The air-gun and water-gun acoustic signals were also observed with two separate calibrated hydrophones (Geospace Model MP24) suspended directly from the crane boom at 3-m depth below each gun. This hydrophone configuration provided a stable, zero-time reference relative to the seafloor that allowed real-time summing of the seismic records observed for the several shots fired at each seismometer clamping depth position.

A special effort was made to reduce the downhole seismic noise caused by the drill pipe and logging cable slamming against the borehole wall. This was done by locking the bottom of the pipe string into the seafloor reentry cone with a casing landing/running tool (CLT) (Fig. 107). With the pipe immobilized, the special high-capacity, precision heave compensator in the drillship's derrick was able to isolate the ship's motion from the downhole pipe string and logging cable. To further reduce pipe/cable slamming noise for the Leg 111 VSP experiment, the rotary bushing was lifted 3 m above the drill rig floor and attached to the immobilized pipe string. This provided additional clearance around the stationary pipe string and moving rig floor. Also the ship's heading was adjusted to minimize roll. These combined measures appeared to markedly reduce the ship-generated pipe/cable slamming noise observed downhole, as will be discussed later.

Experimental Procedure

Prior to locking the drill pipe in the reentry cone, several air-gun and water-gun test shots were recorded with the seismometer clamped in the same physical position at various depths, during pauses as the WST seismometer was initially being lowered (40 m/min) down the borehole. That is, the seismometer clamp was not disturbed between firing the air-gun and water-gun shot sequences. This was done not only to exercise the sound sources before the actual experiment but to provide a series of test shots to compare the S/N ratios for shots observed with the drill pipe unlocked and for shots to be observed later during the actual experiment at the same approximate depth positions with the pipe locked in the reentry cone. Also, at the bottom of the borehole, several test shots were recorded from the same clamping position with the pipe unlocked and then locked.

The VSP experiment commenced with the seismometer deployed to the bottom of the borehole. The drill pipe was first locked into the reentry cone with the CLT, and the heave compensator was engaged. The seismometer was then clamped in the borehole and the logging cable was slacked 3–5 m to help reduce cable slamming noise in the drill pipe. We had also planned to use the logging winch wireline heave compensator to further reduce cable noise, but the compensator failed just prior to the VSP experiment. In any event, after it was ascertained that the seismometer was securely clamped to the borehole wall, the air gun was then fired several times at approximately 25-s intervals. Next the water gun was fired in a similar manner at approximately 15-s intervals. Typically, 10–12 air-gun or large water-gun shots were fired in order to obtain 7 traces deemed to have an adequate S/N ratio for summing into the stack trace at each clamping depth position. However, the small 80-in.^{3} water gun usually required 20 or more shots to obtain the requisite 7 "good" shots. Following the air-gun/water-gun shooting sequence, the WST seismometer was then unclamped and raised 10 m (nominal), and the clamping/shooting procedure was repeated every 10 m up the hole. In the cased portion of the borehole in the sediments (0–274.5 mbsf or 3474–3748.5 mbrf), attempts were made to clamp the seismometer at depths which the sonic logging showed rigid cement bonding of the casing to the borehole sidewall. For a discussion of the cement bond logging results, see "Introduction and Explanatory Notes" chapter, this volume.

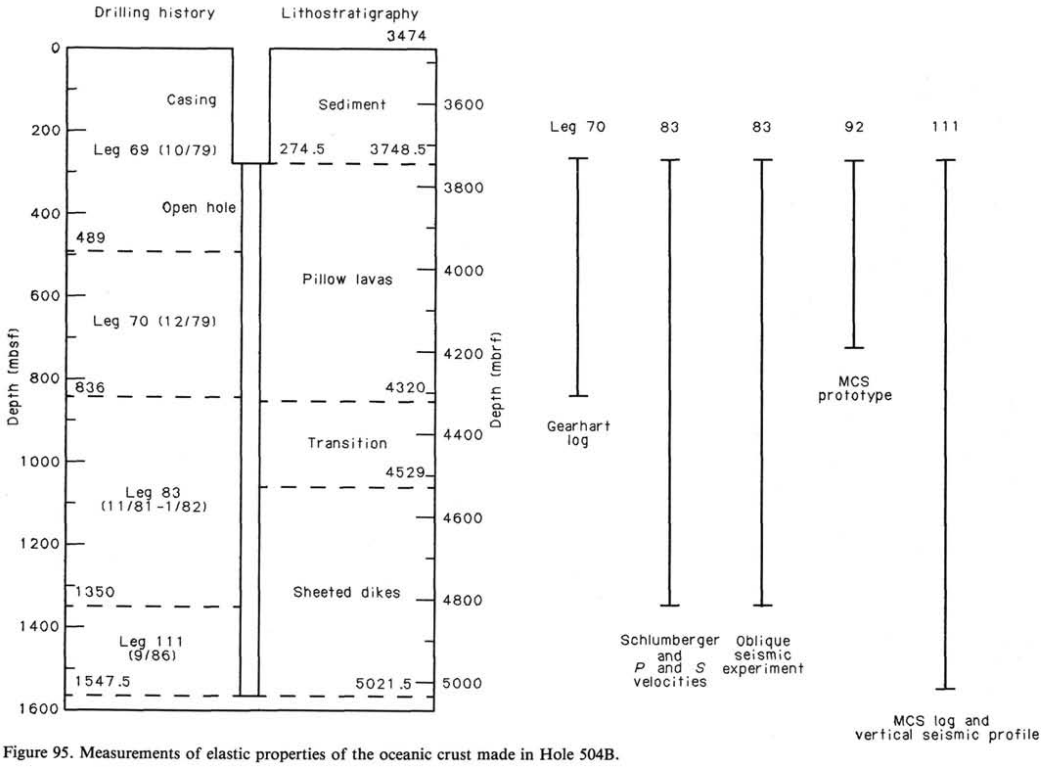

Figure 95. Measurements of elastic properties of the oceanic crust made in Hole 504B.

Data Acquisition

The air-gun/water-gun-generated signals received by the WST borehole seismometer were pre-amplified downhole, transmitted up the the logging cable and digitally recorded along with the hydrophone signals by the PDP-11 minicomputer and A/D converter of the Schlumberger CSU Logging Data acquisition system. Timing information was logged with millisecond accuracy. First break transit traveltimes were calculated to 0.1 ms from the seven shots summed at each depth position. The data sampling rate was 1 ms with a data record length of 3.0 s. The record delay (blanking time) ranged from 2.5 s at the maximum observation depth (1534 mbsf) to 2.2 s at the shallowest depth (330 mbsf). Also the shot number and geophone depth for each shot were digitally recorded.

The seismogram waveforms recorded for each shot were displayed in quasi-real time a few seconds after the shot on a TEKTRONIX graphics oscilloscope. Also the normalized "stack" trace resulting from the summing of the several shots selected for stacking at each clamping depth position was displayed.

Data Processing

Shipboard seismic processing of the VSP data utilized the same PDP-11-based Schlumberger CSU computer system that acquired the field data as well as the ODP underway geophysics MASSCOMP computer with its UTIG-developed HIGHRES/PROCESS seismic processing software. The UTIG MASSCOMP and VAX/DISCO seismic computer systems will be used for post-cruise processing. The CSU system's Seismic Quick Look (SQL) software performed the primary data editing and the preliminary processing tasks while the MASSCOMP system was used for advanced processing and final data display. A summary of the optimum processing sequence is outlined below. However, due to unavoidable delays in developing software to convert the proprietary Schlumberger LIS format field data tapes to SEG-Y exchange data format for processing with the MASSCOMP and other computers, the SEG-Y data conversion step listed below was actually performed after all SQL preliminary processing was completed:

1. Separation of air-gun and water-gun field data records from the shot sequential 800 bpi Schlumberger LIS format data tapes into multiple files of depth sequential data tapes.
2. Conversion of the Schlumberger LIS format data tapes into 1600 bpi SEG-Y format exchange format data tapes for independent use of the MASSCOMP and other computer systems.
3. Post-experiment editing to eliminate or add shot data records from real-time, field-summed stack trace at each clamping depth position. Re-sum good data records to obtain final stacked trace for each depth position.
4. Combine all final stacked traces into composite depth sequential, one-way traveltime trace ensemble after applying static shift correction to account for record delay (blanking) time.
5. Apply static shift correction equal to first break time of the direct wave for each stacked depth trace to align the reflec-

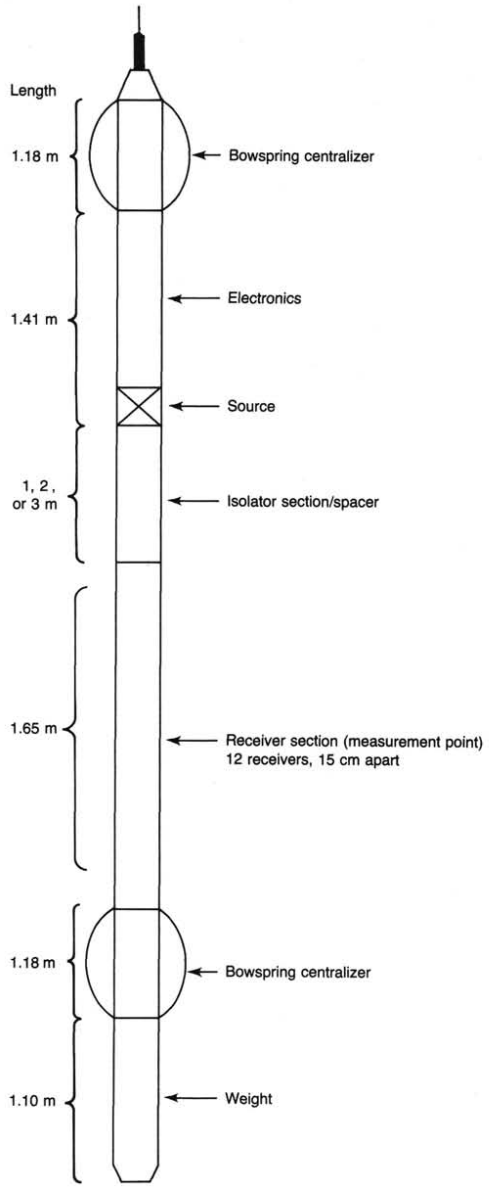

Figure 96. Schematic of the MCS logging sonde.

tion wavetrain pattern along constant arrival times. This results in a composite, two-way traveltime depth trace ensemble.

6. Calculation of velocity-depth profile from time differences of the direct wave first break transit times for various depth intervals.

7. Preliminary wavefield separation into upgoing (reflection) and downgoing (direct) waves using spatial velocity filtering.

8. Perform preliminary source deconvolution using single operator derived from the downgoing waveforms of the deepest four stacked depth traces.

The above preliminary data processing steps were done immediately following the field experiment. Complete analysis and scientific interpretation will require more extensive computer processing for the final wavefield using F-K velocity filters, source wavelet deconvolution, temporal filtering, data archiving, and enhanced graphic display techniques.

Results

The VSP experiment began near the bottom of the Hole 504B borehole at 5009 m below the rig-floor kelly bushing (mbrf), 4998 mbsl, or 1535 mbsf at 0700 on 27 September 1986. The water depth was 3463 m. The borehole total depth of 1547.5 mbsf at the commencement of the VSP experiment could not be reached due to the accumulation of loose rock debris and several roller cone bits lost during the drilling operation just prior to the experiment. Also, subsequent drilling after the experiment deepened Hole 504B to 1562.3 mbsf.

During the 44-hr operations period of the experiment the seas were moderate with 1-m waves and a 2–3-m swell. The drill-floor heave was estimated to be about 1 m (20 s period) with a maximum roll of 2°. Pitch was negligible.

A total of 180 seismometer clamping positions were occupied utilizing about 34 hr of total recording time. After an initial start-up delay to attempt to repair a malfunction in the 400-in.^{3} water gun, less than 10 min on average were usually required for observations at each clamping depth position.

Approximately 6 hr were required to deploy and recover the WST seismometer.

As noted earlier, approximately 2 hr were lost due to the failure of the 400-in.^{3} water gun at the VSP experiment's first clamping depth position (1535 mbsf). The unit had to be repaired using some makeshift O-rings, since the proper O-ring spares were not on hand due to mislabeling of the shipboard spares package. Unfortunately, the hastily repaired water gun failed again, and a much smaller 80-in.^{3} unit had to be substituted. This was the only equipment malfunction noted during the experiment; however, the outermost, hardened steel rock-gripping tooth on the upper arm of the WST seismometer unit was found to be missing on conclusion of the VSP experiment (3638 mbsl) at 0300 on 29 September 1986.

Downhole Noise Levels

Inspection of the true amplitude seismograms recorded for several air-gun shots with the drill pipe unlocked (Fig. 112) and locked (Fig. 113) in the reentry cone shows that very high signal-to-noise levels can be achieved by using the drill pipe immobilization procedure described above. For these comparisons all shots were recorded during a single clamping of the seismometer in the borehole. The noise reduction advantage of the CLT locking appears to be greater the closer the seismometer clamping depth position is to the bottom of the drill pipe (Figs. 114 and 115, respectively). In fact, after summing the seven shots typically included in each depth stack, it is estimated from comparison of the direct wave first break amplitudes with the background noise level that a S/N ratio of +40 db was observed for the large 950-in.^{3} air-gun shots (Fig. 116). However, comparison of the S/N ratio for 400-in.^{3} water-gun and 950-in.^{3} air-gun shots recorded at and during the same clamping depth position showed the water-gun shots to have a somewhat lower S/N ratio (Fig. 117). The small 80-in.^{3} water gun showed even lower S/N ratios compared to the air-gun shots (Fig. 118). Its S/N ratios were still generally less than 20 db after firing as many as 20 shots at each clamping depth position. The increased time required to record the small water-gun shots necessitated suspen-

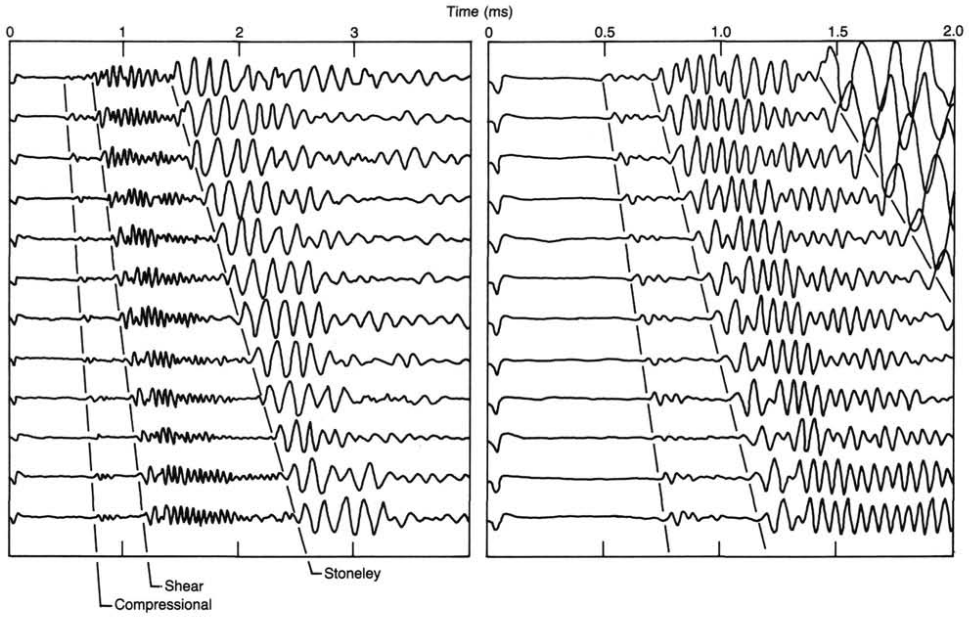

Figure 97. Sample waveform suite from unfractured granodiorite, showing the different arrivals expected in hard rock.

sion of water-gun VSP observation over the mid-range depth interval between 1296 and 526 mbsf.

Tool Resonance

Figure 119 shows a comparison of air-gun and water-gun shots recorded at the same clamping depth position where the borehole diameter was relatively large (> 13 in.). Note the high resonance of the water-gun shot (~ 100 Hz) as compared to the air gun. In general, the air gun excited much less resonance noise in the WST tool, even in the largest borehole diameters encountered in Hole 504B (14.9 in.). Clearly, the WST tool appears to be susceptible to high-frequency resonance (~ 100 Hz) in borehole diameters greater than 12 in.

How much the loss of the upper clamping arm's outermost tooth during the experiment contributed to the WST resonance noise is difficult to estimate since the depth where the loss occurred is not known. However, inspection of the raw air-gun seismograms (Fig. 120) reveals that even this gun exhibited increased resonance beginning at depth 4294–4199 mbsl, as the seismometer was raised up the borehole. Unfortunately, this observation is not conclusive since the borehole diameter was generally larger in the upper part of the borehole. In any event, it appears the tooth was certainly lost by the time of the observation made near the end of the VSP experiment in the cased portion of the borehole. Here reoccupation of the same approximate clamping depth positions, used during the initial lowering of the WST seismometer, was not always possible. The tool appeared to slip down the casing a few meters before it could be rigidly clamped to the sidewall.

Vertical Seismic Profile Results—Air Gun

Figure 120 shows the one-way traveltime, stacked depth trace ensemble of all the raw air-gun-shot VSP seismograms acquired at Hole 504B over the depth interval 1535–164 mbsf (4998–3627 mbsl). Note the drill pipe bottom was at 145 mbsf (3629 mbrf), which prevented shallower seismometer clamping.

The depth trace ensemble includes 129 observations made in the uncased, open borehole in Layer 2 as well as 7 observations made in the cased borehole through the overlying sediments and uppermost volcanic basement rocks between 164 and 286 mbsf (3749–3627 mbsl). The seismograms are unfiltered. However, a spreading loss-type, 1.5-power exponential time gain factor has been applied in order to display the weaker, deep reflections. Each trace amplitude scale is normalized.

The downgoing, direct waves are the strong first arrivals sloping downward to the right in Figure 120. Note the direct wave's bubble pulse arrival wavetrain which parallels and trails the first break arrivals by about 180 ms. Note that no water bottom multiple arrivals were recorded in this experiment because the one-way traveltime through the water column is 2300 ms. The three-way traveltime (6900 ms) for a VSP-type, water bottom multiple is well beyond the maximum data record length of this experiment (i.e., 5500 ms for a 3000-ms data record and a 2500-ms delay).

The upgoing, reflected waves are the very weak events forming an arrival wavetrain pattern that slopes upward to the right in Figure 120. The amplitude of these reflected waves is probably − 40 db less than the direct waves which is typical for VSP experimental results. Potential reflection arrivals are labelled *R* and are best seen by holding the page level and viewing the figure from a low angle. The divergence of the upgoing and downgoing wavefields is more apparent in the upper part of the enlarged version of the the 2400–3900-ms portion of the VSP depth-trace ensemble shown in Figure 121. Here several potential reflection wavetrains are indicated by their respective arrow pairs E_1, E_2, E_3, E_4, E_5, and X. This divergent arrival pattern re-

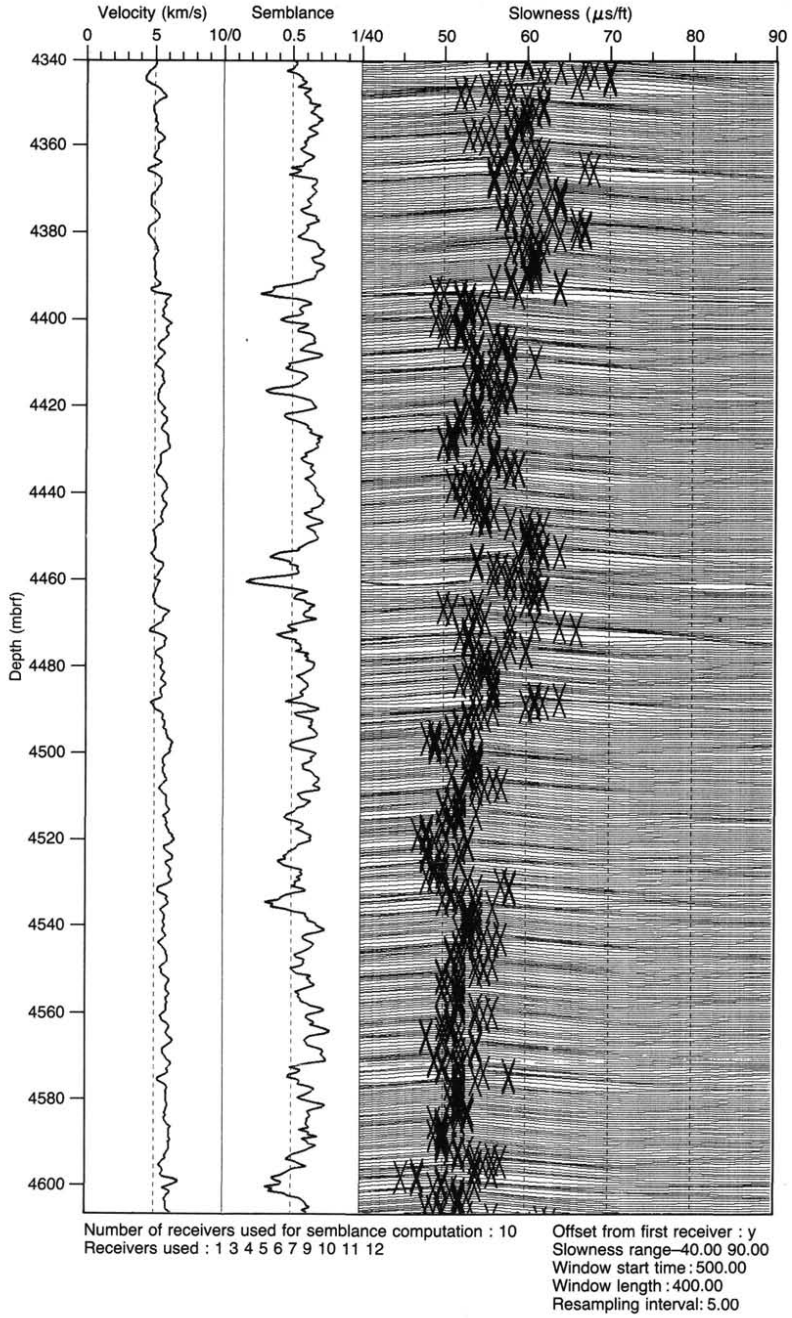

Figure 98. Example of compressional velocity determination from semblance computation of data acquired during the second MCS run of Leg 111 in Hole 504B.

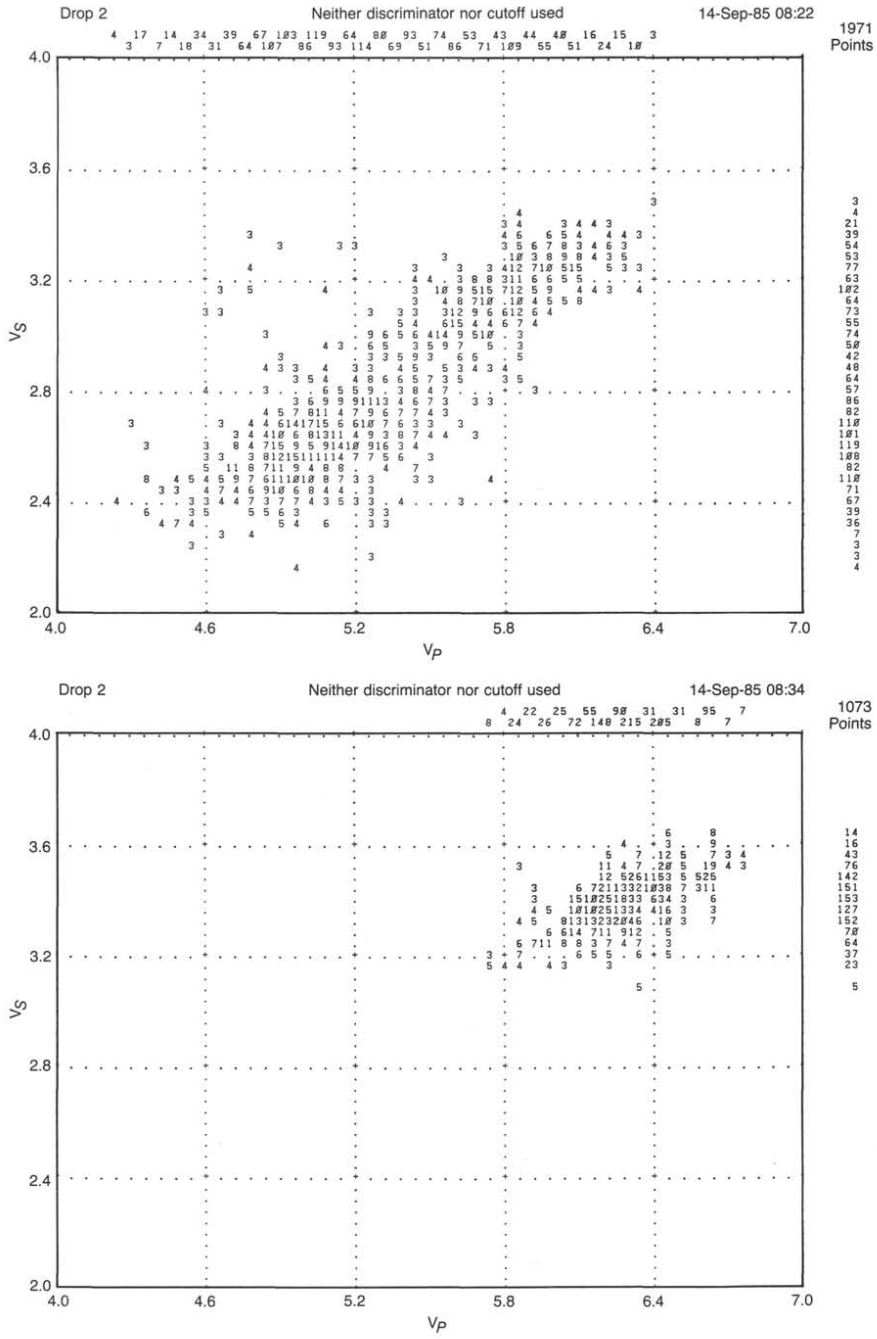

Figure 99. Plot of V*p* vs. V*s* for Layer 2A and 2B (3760–4420 mbrf, 286–946 mbsf) (top), and Layer 2C (4420–5000 mbrf) (bottom).

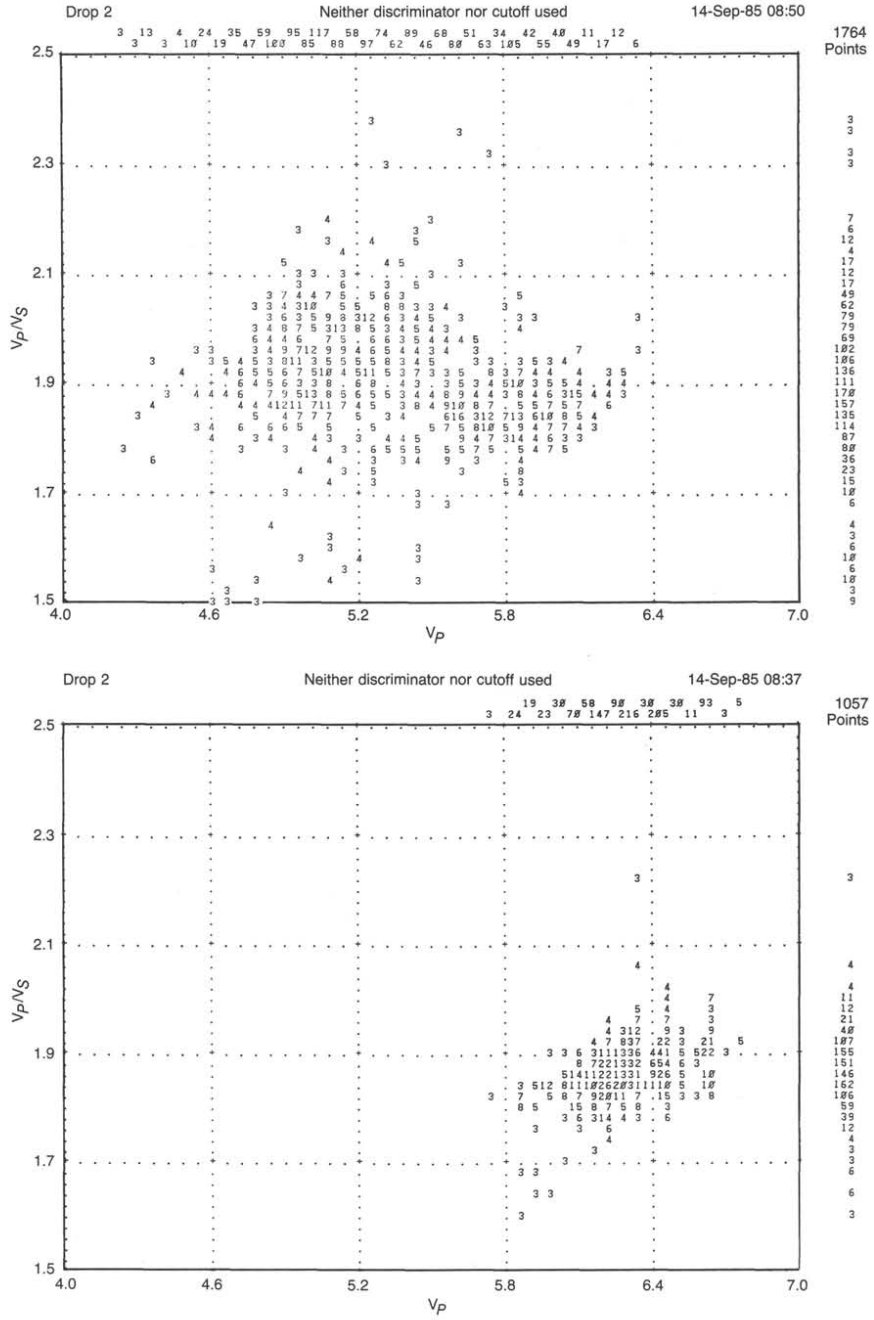

Figure 100. Plot of V*p* vs. V*p*/V*s* ratio for Layer 2A and 2B (3760 m–4420 m, 286–946 mbsf) (top), and Layer 2C (4420–5000 m, 946–1526 mbsf) (bottom).

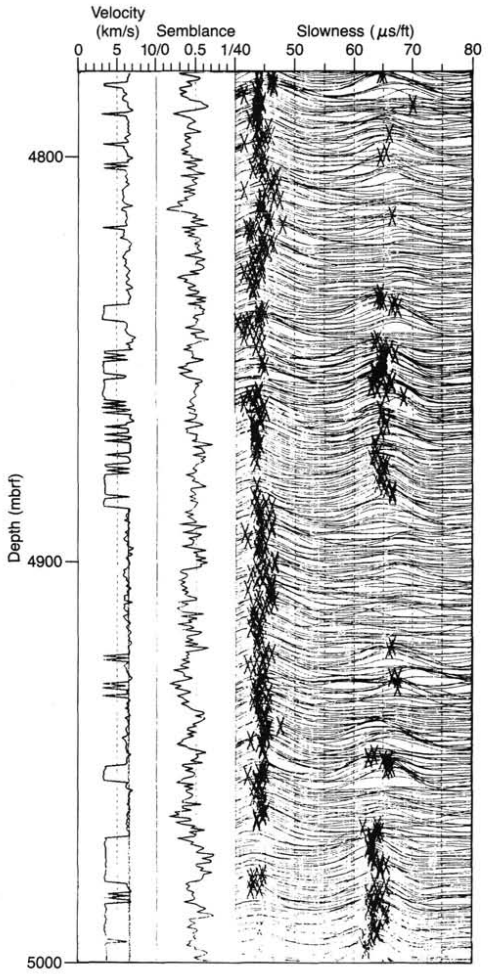

Figure 101. Slowness computation from semblance computation on 4800–5000 m in Hole 504B. The processing covers both compressional and shear arrivals.

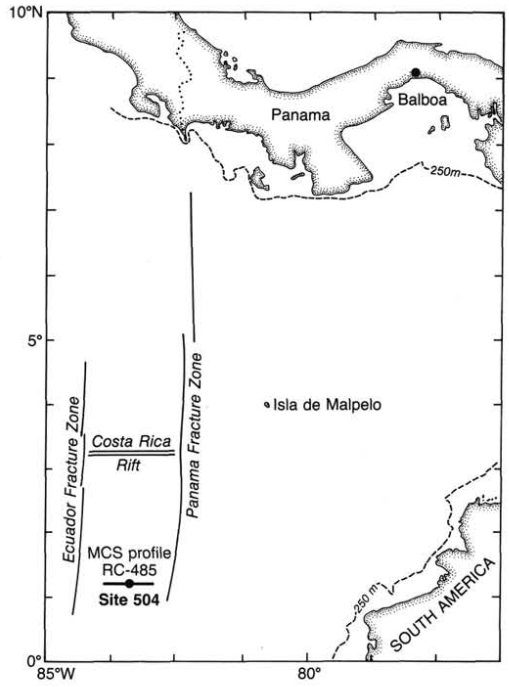

Figure 102. Location map showing Site 504 and multichannel seismic (MCS) profile RC-485. Bathymetry in meters.

sults from the decreasing range to the sound source for the direct waves and the increasing range from the reflecting interface as the seismometer is raised to shallower borehole depths as depicted in Figure 103. Note that the reflected wavetrains should intersect the direct wave's first break arrival wavetrain at the depth of the interface causing the reflection.

Vertical Seismic Profile Results—Water Gun

Figure 122 shows the two-way traveltime, stacked depth trace ensemble for all the raw, water-gun-shot VSP seismograms acquired during Leg 111 at Hole 504B over the depth interval 4938–3624 mbsl. The major gap in the depth coverage between 4759 and 3989 mbsl (1296–526 mbsf) was caused by the intentional cessation of water-gun shooting due to the excessive time required to obtain seven "good" shots with adequate S/N ratio for summing into each depth trace stack. Note that the data display parameters in Figure 122 are the same as those used for the raw air-gun ensemble shown in Figure 120. Although the water-gun seismograms appear to have a lower S/N ratio and exhibit more high-frequency resonance, the depth trace ensemble shown in Figure 122 indicates that useful water-gun information was acquired. Unfortunately, the brevity of the post-experiment period available for preliminary computer processing and analysis do not allow further consideration of the water-gun results at this time.

Discussion

Downgoing Direct Waves

A preliminary determination of the interval velocity-depth structure at Site 504 can be made simply by dividing the interval distance between various seismometer clamping depth positions by the difference in their direct wave first break arrival traveltimes (Mons and Barbour, 1981). Figure 123 shows the observed borehole traveltime curve (left) and the calculated interval velocity-depth profile calculated using this method from the seafloor down to 1535 mbsf (3463–4998 mbsl). The seismometer depth separation intervals selected were typically 20 m but ranged from 15 m to 50 m. The traveltime (104 ms) through the sediments between the seafloor and the shallowest seismometer clamping depth (164 mbsf) was computed by taking the difference between the traveltimes observed with the *Resolution*'s 12-kHz echo sounder and the borehole seismometer. The traveltimes to the depths for the boundaries of the various seismic velocity and

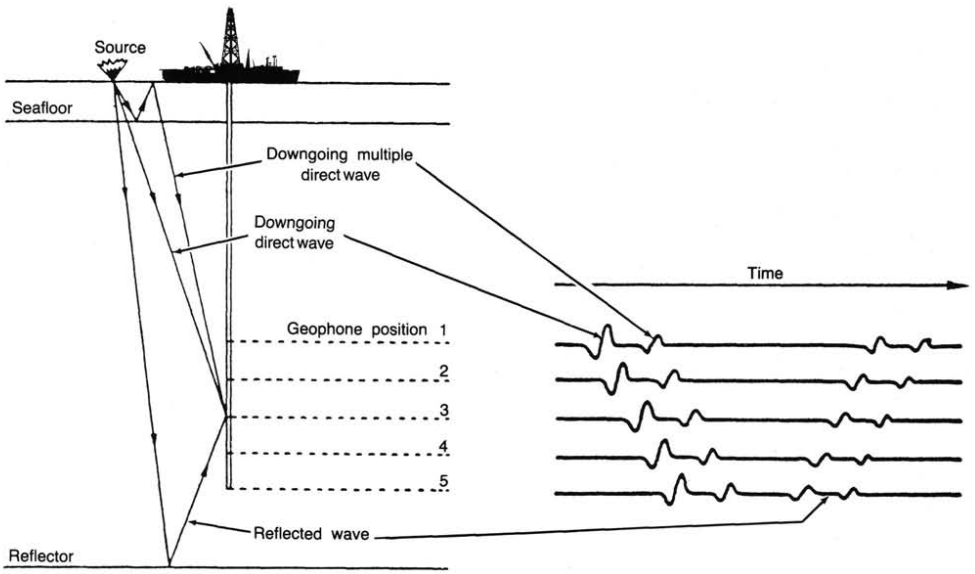

Figure 103. Schematic representation of ray paths and wavetrain arrival pattern for a marine vertical seismic profile (VSP) experiment (modified after Mons and Barbour, 1983).

lithologic units recognized in Hole 504B (Salisbury et al., 1985; Becker, 1985) have been interpolated from the observed borehole traveltime curve and are shown at the right in Figure 122. Table 35 presents a summary of the VSP-derived interval velocities for each seismolithologic unit.

Sonic logging velocity profiles have previously been reported for Hole 504B from DSDP Legs 83 and 92 logging data by Salisbury et al. (1985), Mutter and Newmark (1986), and Moos et al. (1986). Comparison of the VSP interval velocity-depth profile with the DSDP Leg 83 sonic profile shows good general agreement. However, the wide excursions seen in the DSDP Leg 92 sonic velocity profiles, especially those ranging from 2000 to 7000 m/s described by Moos et al. (1986) for thin units within the uppermost part of Layer 2A, cannot be verified. This might be expected due to the much wider spacing of the VSP observations compared to the sonic velocity logging measurement interval (i.e., 10 m vs. 0.15 m, respectively). Further VSP data comparisons with the new sonic velocity logging results obtained on ODP Leg 111 (see "Multichannel Sonic Log" section, this chapter) as well as the oblique reflection/refraction results recently reported by Little and Stephen (1985) and Stephen and Harding (1983) for Hole 504B will be an important part of future shore-based studies.

Upgoing Reflected Waves

Full interpretation of the reflected wavefield observed in VSP experiments requires careful separation of the the upgoing and downgoing waves using velocity filtering (Seeman and Horowicz, 1983). Deconvolution of the upgoing reflected waves is done using the downgoing, direct wave of each seismogram to derive a source wavelet operator (Lee and Balch, 1983). Iterative modeling techniques are commonly employed to match synthetic seismograms computed from borehole logging/physical properties information with the observed VSP reflected wavefield (Grivelet, 1985). The VSP reflection seismogram can also be compared with the surface ship MCS reflection profile which crosses the borehole site (Poster, 1983). This allows extrapolation of the borehole coring and logging information over the region surrounding the drill site.

Although such detailed analysis of the reflected wavefield is clearly beyond the scope of this field data report, certain qualitative inferences can be made about the reflected waves from the preliminary wavefield separation procedure initiated during the Leg 111 cruise:

1. First, each seismogram of the partial one-way traveltime, stacked depth trace ensemble (Fig. 121) was static-shifted by the time of the direct wave's first break arrival. The time shifting results in the 4900–6400-ms two-way traveltime seismogram ensemble shown in Figure 124. This time-shift serves to align all wavetrain arrivals reflected from simple, single horizon planar interfaces along the vertical, two-way traveltime axis of the figure. Note also that the visual alignment of the reflection wavetrains is markedly enhanced by this simple time-shifting and is again best seen by holding the figure level and viewing it from a low angle. In fact, many of the weak reflections (E_1–E_5, X) only tentatively identified in the one-way traveltime plot of Figure 121 can now be confidently traced in Figure 124.

2. Next, a spatial velocity filter was applied to the partial two-way traveltime seismogram ensemble shown in Figure 124 to reject all dipping wavetrains and thus enhance the reflected arrival wavetrains along the vertical time axis. The result of this preliminary attempt to separate the upgoing reflected wavetrains arriving during the initial 1000 ms of the two-way traveltime seismogram ensemble is shown in Figure 125. Ideally, the upgoing arrivals would present a pattern of nearly vertical isochronous wavetrains if the reflecting interfaces are simple horizontal planes. In fact, careful examination of Figure 125 reveals that while most of the weak, high-frequency wavetrain arrivals are indeed aligned along vertical isochron lines, especially at the top

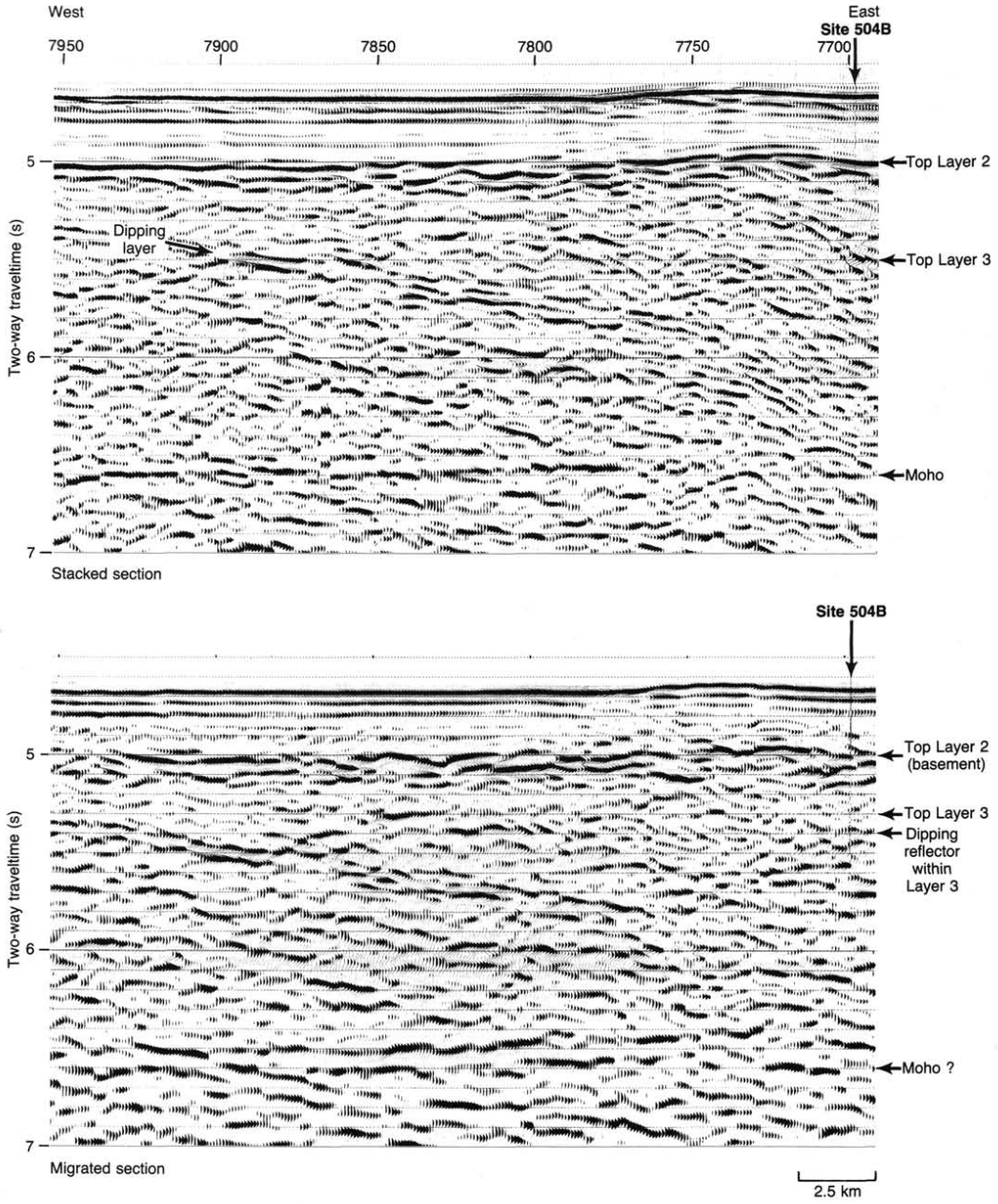

Figure 104. MCS profile RC-485. Top profile is the conventional common depth point (CDP), 24-fold stacked section showing anticipated 2000 m depth of total penetration projected after the Leg 111 drilling at Hole 504B. This assumed an average velocity of 5.5 km/s for the upper part of Layer 2. The actual depth of penetration was 1562 mbsf and two-way traveltime of 5.43 s (profiles provided by J.M. Mutter and T. Brocher, respectively; pers. comm., 1986).

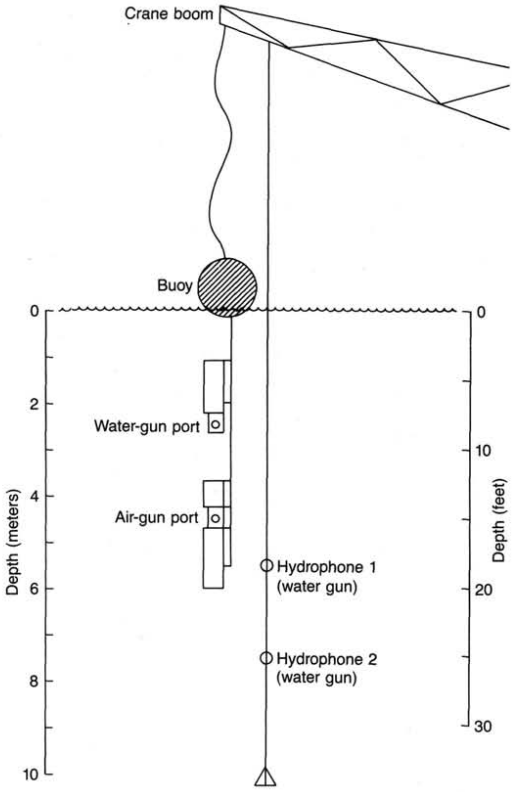

Figure 105. Schematic drawing of the air-gun/water-gun sound source array and hydrophone receivers used for the Leg 111 vertical seismic profile (VSP) experiment.

of the borehole, the strongest reflection wavetrains are low-frequency events, labeled X, Y, and Z in Figure 125 which appear to curve to the right toward the bottom of the figure (borehole). Significantly, the weak, isochronous high-frequency wavetrain E_5 can be traced upward from the bottom of the borehole and appears to coalesce with the strong, curved wavetrain X above a depth of 4000 mbsl.

3. The curved aspect of wavetrain X, as well as the other curved events, labelled Y and Z in Figure 125, probably result from reflections emanating from dipping planar interfaces not directly beneath the borehole axis as shown in Figure 126 (Kennett et al., 1980; Kennett and Ireson, 1981). This curvature can be useful for calculating the true dip of these interfaces in that reflection wavetrain arrivals from a dipping interface will, in general, present a leftward (upward) convex, hyperbolic traveltime curve. The amount of hyperbolic move out relative to the distance moved by the seismometer in the borehole is proportional to the dip (Kennett et al., 1980). The arrivals will appear to move out from the intersection point of the equivalent horizontal reflector's traveltime curve with the direct wave's traveltime curve (Fig. 126).

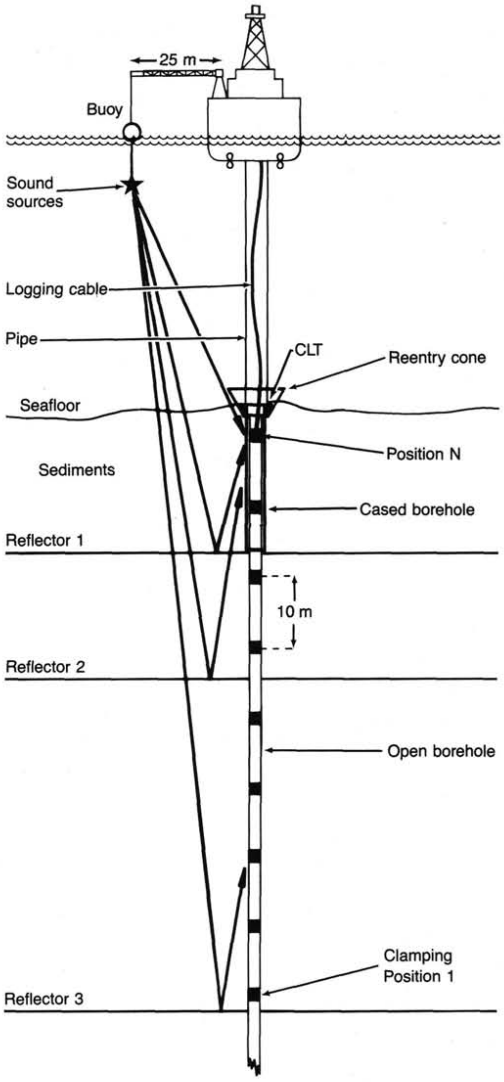

Figure 106. Vertical seismic profile (VSP) experiment configuration at Hole 504B. Downgoing direct and upgoing reflected ray paths are shown for multiple seismometer clamping depth positions. Note that the offset of the sound sources is exaggerated in order to illustrate clearly the various ray paths. The casing landing tool (CLT) is shown locked in the borehole reentry cone on the seafloor.

Preliminary Geologic Interpretation

The observed borehole depth of the VSP measurements of two-way traveltimes to the various seismic and lithologic units recognized in Hole 504B are summarized in Table 36. The unit

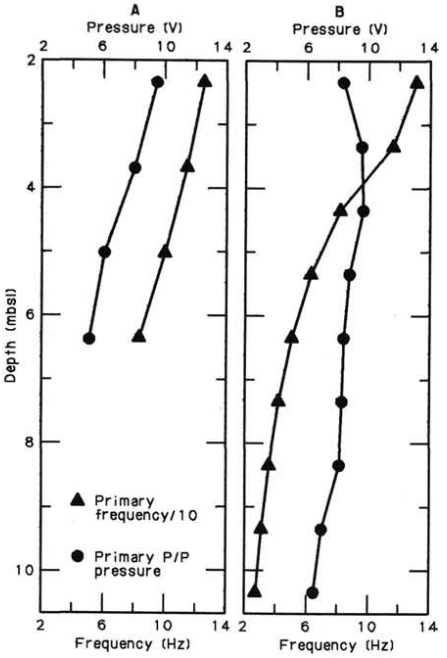

Figure 107. Source pulse variation with depth. A. Using 400-in.^{3} water gun. B. Using 487-in.^{3} air gun with debubbler. Primary pulse peak pressure (peak to peak = p/p) and frequency (Hz). The hydrophone calibration was 18 V/bar, and its distance from the source was maintained at 3 m for all test firing depths.

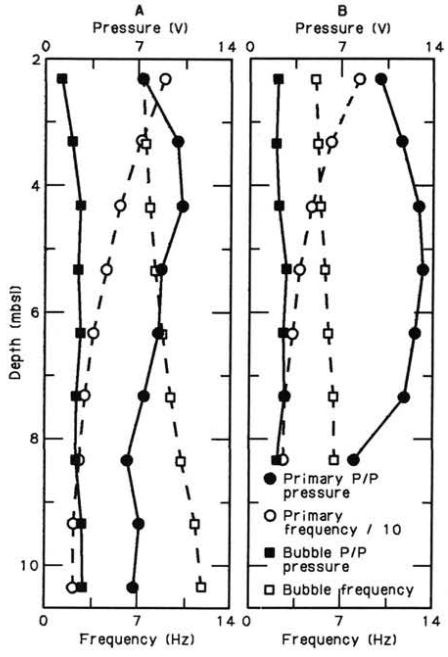

Figure 108. Source pulse variation with depth. A. Using 300-in.^{3} air gun. B. Using 950-in.^{3} air gun without debubblers. Primary peak pulse (peak to peak = p/p) and frequency (Hz). Also shown is the bubble pulse peak pressure and the primary/bubble frequency.

boundaries are also shown to the right in the preliminary VSP reflection seismogram of Figure 127. The reflection wavetrains E_1-E_5 and X are indicated by arrows and labeled on the left of Figure 127. Close inspection of this figure reveals that several of the unit boundaries seen in the borehole closely correlate with observed reflection wavetrains. Specifically the tops of Layer 2B, transition zone, sheeted dikes, and Layer 2C appear to coincide with reflectors E_1, E_3, E_4, and E_{41}, respectively. The two VSP reflection wavetrains E_2 and E_{42}, seen at 566 and 1456 mbsf, can not be correlated with any major seismolithologic boundaries to date in Hole 504B.

The curved reflector X is the strongest VSP reflection arrival observed in Figure 127. This wavetrain may be a reflection from the uppermost of the dipping reflector 3 sequence whose top is seen at about 5700 ms (5.7 s two-way traveltime) in the migrated MCS profile which crosses Site 504 (Fig. 104, bottom). Similar dipping reflector sequences have been observed in the lower part of Layer 3 along wide-aperture MCS profiles in the northwest Atlantic (NAT Study Group, 1985). There they are believed to be indicative of layer cumulate structures resulting from magnetic differentiation processes at the ridge axis. Accordingly, if the two-way traveltime to the deepest seismometer clamping depth (1535 mbsf) is 5422 ms (two-way traveltime), the traveltime to the top of the Layer 3 dipping reflectors at Hole 504B, as seen in Figure 104, would be an additional 278 ms. Also, the weak high-frequency reflector E_5 which arrives at 5460 ms or 38 ms beyond the traveltime to the deepest seismometer depth (1535 mbsf) may mark the next major horizontal reflection interface directly beneath the borehole. Assuming a velocity of 6500 m/s, the depth to these potential Layer 3 reflection horizons is estimated to be 903.5 and 123.5 m, respectively, beyond the deepest seismometer clamping depth or 2438.5 and 1658.3 mbsf, respectively.

Conclusions

A vertical seismic profile using a large air-gun sound source aboard the *JOIDES Resolution* has provided the velocity-depth structure and reflection seismogram for the oceanic crust and the upper mantle at Hole 504B. Comparison of the VSP reflection seismogram with the borehole lithology, well logging data, and surface ship MCS profiles indicates that moderate resolution (say ± 10 m) correlations of deep reflectors can be made to determine the regional geologic framework for Hole 504B. Unfortunately, failure of the large, high-frequency water-gun source originally planned for this VSP experiment may have compromised our objective to obtain higher resolution reflection data from the lower crust.

MAGNETOMETER LOG

Introduction

This report describes some experimental problems in magnetometer logging. Results of the magnetometer log in Hole 504B yield important information regarding a vertical tectonic rotation exceeding 10° in the upper part of the crust. The log data are compared with paleomagnetic data from this hole, and with past magnetometer logs in Holes 395A, 501, 504B, and 505B.